Progress In Electromagnetics Research, Vol. 111, 119–139, 2011

FAST COMPUTATION OF THE FORWARD SOLUTION IN CONTROLLED-SOURCE ELECTROMAGNETIC SOUNDING PROBLEMS

M. Parise

Faculty of Engineering, University Campus Bio-Medico of Rome
Via Alvaro del Portillo 21, 00128 Rome, Italy

Abstract—The forward problem of calculating the electromagnetic (EM) field of a circular current loop in presence of a layered earth structure, given the geometrical and EM parameters of the layers, is solved fast. Efficient computation is obtained through a quasi-analytical procedure that allows to transform the field integrals into expressions involving only a known Sommerfeld Integral. The final explicit forms of the fields are in terms of modified Bessel functions. To validate the method, the magnitudes of the EM field components versus induction number and versus frequency are calculated assuming two- and three-layer earth models. The achieved results are in good agreement with the ones provided by the commonly used digital filter algorithms. The computational time taken by the application of this technique is shown to be much less than that required by both digital filters and other recently developed integration techniques for similar problems. This paper is an extension of an earlier conference paper.

1. INTRODUCTION

The controlled-source electromagnetic (CSEM) sounding method consists of acquiring information about the subsurface structure of a layered earth medium by measuring the EM fields produced above its surface by an intentional source [1–8]. Information may be the thicknesses or the EM properties of the various layers. One way to collect CSEM data is to measure the frequency-domain EM coupling between a transmitting and a receiving insulated wire loop at a set of discrete frequencies, typically spanning several decades [2, 3, 5, 6, 8, 9].

Received 14 October 2010, Accepted 25 November 2010, Scheduled 1 December 2010
Corresponding author: Mauro Parise (m.parise@unicampus.it).

The objective is then to solve the nonlinear inverse problem of searching for a layered earth model that can acceptably reproduce the recorded finite set of observations.

Conventional iterative solution algorithms for nonlinear inverse problems require to solve a number of forward problems within an optimization loop (as an example, see the Levenberg-Marquardt method [10, 11]). This is the reason why the problem of the fast and accurate calculation of the EM field generated over a layered earth structure by a large circular loop source has attracted the attention of scientists since the inception of EM prospecting methods [1–5]. In particular, several recent papers document an extensive usage of the digital linear filter technique for numerically evaluating the integral expressions for the EM field components [3, 7, 12, 13]. The major drawback of such technique is that it ensures high computational accuracy only when the filter operator is an ad-hoc filter, that is its coefficients (the weights and the sampling interval) are tailored to the function to be transformed [12–14]. In other terms, a filter may produce error-free or inaccurate results depending on whether it is applied to one transform or another. What is typically done to overcome this problem is to run an optimization algorithm which, especially when designing very long filters, may take considerable time [13].

An attempt to avoid the use of digital filters for evaluating similar integral transforms has been made in [15], where a highly accurate integration method based on the pole-residue approximation of part of the kernel function has been presented. This method has the advantage of being always matched to the specific transform to be calculated, but every execution of it takes at least 8 seconds on a 1.6 GHz PC. Since it is required one execution per frequency value, the method is not recommended in the case of multi-frequency applications like the frequency-domain CSEM sounding method, while it fits optimally to single-frequency problems like that described in [15].

This paper introduces an efficient procedure for fast computing the spatial distributions of the EM field components produced by the loop source. Starting from the pole-residue approximation of the parts of the integrands that do not depend on the distance from the loop axis, in a similar fashion as discussed in [15], the field integrals are cast into forms involving uniquely a known tabulated Sommerfeld Integral. The radial distributions of the EM field components at a height z above the medium are explicitly provided as linear combinations of modified Bessel functions of the first kind (for in-loop observation points) or second kind (for offset points).

The proposed technique inherits the advantages of the previously

developed method of calculation of integral transforms based on the rational function-fitting of the kernel functions. This means that it is not tailored to a particular integral rather than another one, and it allows the user to specify the desired accuracy of the numerical results within the machine precision. What is more, the new integration procedure does not require the poles of the rational approximations to have negative real part. This feature is what makes it possible to realize an enormous speed increase with respect to the previous pole-residue based approach [15], which forces the fitting algorithm to calculate new sets of poles and residues every time one or more of the generated poles have positive real part.

Numerical applications are performed in order to validate the new technique. The achieved results are in fairly good agreement with the data provided by the digital filter formulation presented in [12].

It must be highlighted that the object of this research is to offer a method for the high-speed computation of the forward solution, which necessarily translates into a significant reduction of the execution time of any iterative inversion algorithm [16–25]. Detailed considerations about the inversion process itself or comparative evaluations of various inversion techniques are outside the scope of this paper. The present article is a revised and extended version of a previous conference paper [26].

2. FORMULATION

Consider a current-carrying circular loop lying on the surface of an M-layer medium. The geometrical dimensions, the EM parameters, the loop current are as depicted in Fig. 1.

The frequency-domain integral expressions for the generated EM field components at an observation point (ρ, φ, z) in the air region are well known in literature [12, 27–29]. With the time-harmonic factor $e^{j\omega t}$ suppressed for better clarity, they can be written in compact form as

$$E_\varphi = \omega\mu_0 Ia\Phi_{1,1}, \quad H_\rho = -jIa\Phi_{1,2}, \quad H_z = jIa\Phi_{0,1} \tag{1}$$

where

$$\Phi_{h,k}(\rho, z) = \int_0^\infty f^{(k-1)}(z, \lambda) J_1(\lambda a) J_h(\lambda\rho) \lambda^{2-h} d\lambda. \tag{2}$$

In Equation (2), $J_h(\cdot)$ is the Bessel function of order h, while

$$f^{(k-1)}(z, \lambda) = \frac{\partial^{k-1} f(z, \lambda)}{\partial z^{k-1}}, \tag{3}$$

with

$$f(z,\lambda) = \frac{1}{2ju_0}\left[e^{-u_0(t+z)} + R^{TE}e^{-u_0(t-z)}\right], \tag{4}$$

being

$$R^{TE} = \frac{N_0 - Y_1}{N_0 + Y_1} \tag{5}$$

the transverse electric plane wave reflection coefficient R^{TE} at the air-ground interface [30–32]. The surface admittance Y_1 is obtained through the recurrence relation

$$Y_m = N_m \frac{Y_{m+1} + N_m \tanh[u_m(z_m - z_{m-1})]}{N_m + Y_{m+1}\tanh[u_m(z_m - z_{m-1})]}, \qquad m = M-1, \ldots, 1, \tag{6}$$

with

$$Y_M = N_M, \tag{7}$$

while the intrinsic admittance N_m of the m-th layer is given by

$$N_m = \frac{u_m}{j\omega\mu_m}, \tag{8}$$

with

$$u_m = \sqrt{\lambda^2 - \omega^2\mu_m\epsilon_m + j\omega\mu_m\sigma_m}. \tag{9}$$

The conventional approach to evaluate Fourier-Bessel transform of the type (2) is the digital linear filter technique [13]. According to such technique, $\Phi_{h,k}$ may be expressed as [13, No. 3]

$$\Phi_{h,k}(\rho, z) \cong \frac{1}{\rho}\sum_{l=1}^{L} f^{(k-1)}(z, \lambda_l) J_1(\lambda_l a)\lambda_l^{2-h} W_{h,l}, \tag{10}$$

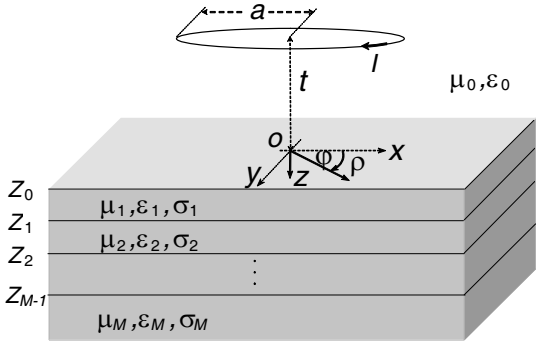

Figure 1. Geometry and coordinates for an M-layer planar medium exposed to the field of a current loop.

where $W_{h,l}(l = 1, \ldots, L)$ is a set of filter weights, and

$$\lambda_l = \frac{1}{\rho} 10^{[a+(l-1)s]}, \qquad l = 1, \ldots, L, \tag{11}$$

is a set of L abscissae along the λ-axis, being a and s respectively the position of the starting point for sampling the kernel function and the sampling interval.

Some drawbacks arise from using (10). First, the weights of a filter are predetermined and, as such, cannot be appropriate for every integral transform [13, 14]. This means that the same set of weights may offer high performances when applied to the computation of particular transforms, and be completely unsuitable for other transforms. Hence, only a theoretical estimation of the precision of a filter operator can be made a priori, the validity of which needs to be further tested case by case.

Second, some authors [13] noticed that it is always possible to enhance the theoretical precision of a filter by increasing its length L, but at the cost of running filter design algorithms that involve time-consuming optimization processes.

The objective of this paper is to present a simple and robust, semi-analytical method for evaluating integrals of the form (2), which responds to the following requirements. First, it must provide highly accurate results regardless of the transform to which it is applied. Such feature allows to overcome the principal disadvantage of digital filter technique. Second, the execution of the method has to take minimum time consumption, and this is because the inversion of CSEM data may require a huge amount of forward problems to be solved.

The first step consists of substituting two pole-residue representations for the even functions $f^{(k-1)}(z, \lambda)$, $k = 1, 2$, which decay without oscillations with increasing $|\lambda|$.

Rational approximations of the form

$$f^{(k-1)}(z, \lambda) \cong g_k(z, \lambda) = \sum_{n=1}^{N_k} \frac{r_{k,n}(z)}{j\lambda^2 - p_{k,n}(z)}, \tag{12}$$

can be easily obtained via the fitting technique described in [33–36], and combined with (2) to give

$$\Phi_{h,k} = -j \sum_{n=1}^{N_k} r_{k,n} \int_0^\infty \frac{J_1(\lambda a) J_h(\lambda \rho)}{\lambda^2 + j p_{k,n}} \lambda^{2-h} \, d\lambda, \tag{13}$$

where the dependences of the quantities upon ρ and z have been omitted for notational simplicity. To evaluate the integral on the right-hand side of (13) it can be made use of the well known result [37, No. 6,

P. 430]:

$$\int_0^\infty \frac{\lambda^{\kappa-1} J_\mu(\lambda\beta)}{\lambda^2+\gamma^2} \left[\cos\psi J_\nu(\lambda\alpha)+\sin\psi Y_\nu(\lambda\alpha)\right] d\lambda = -I_\mu(\gamma\beta)K_\nu(\gamma\alpha)\gamma^{\kappa-2}, \tag{14}$$

valid for $\alpha \geq \beta$ and $\Re[\gamma] > 0$.

Here $Y_\nu(\cdot)$ is the Neumann function, $I_\mu(\cdot)$ and $K_\nu(\cdot)$ are modified Bessel functions of the first and second kind, while $\psi = (\kappa+\mu-\nu)\pi/2$.

When $\rho < a$, the left-hand side of (14) turns into the integral in (13) only if $\alpha = a$, $\beta = \rho$, $\gamma = \lambda_{k,n} = \sqrt{jp_{k,n}}$, $\kappa = 3-h$, $\mu = h$, $\nu = 1$. It follows that $\psi = \pi$, and

$$\int_0^\infty \frac{\lambda^{2-h} J_h(\lambda\rho)}{\lambda^2+\lambda_{k,n}^2} J_1(\lambda a)\, d\lambda = I_h(\lambda_{k,n}\rho)K_1(\lambda_{k,n}a)\lambda_{k,n}^{1-h}. \tag{15}$$

Instead, for $\rho > a$ it must be $\alpha = \rho$, $\beta = a$, $\mu = 1$, $\nu = h$, and, as a consequence, $\psi = (2-h)\pi$. Since h is equal to 0 or 1, Equation (14) becomes

$$\int_0^\infty \frac{\lambda^{2-h} J_1(\lambda a)}{\lambda^2+\lambda_{k,n}^2} J_h(\lambda\rho)\, d\lambda = I_1(\lambda_{k,n}a)K_h(\lambda_{k,n}\rho)\left(-\lambda_{k,n}\right)^{1-h}. \tag{16}$$

Substitution of (15) and (16) into (13) provides

$$\Phi_{h,k}(\rho,z) = -j\sum_{n=1}^{N_k} b_{h,k,n}^{(\gtrless)}(z) C_{h,k,n}^{(\gtrless)}(\rho,z), \tag{17}$$

where the symbols $<$ and $>$ indicate respectively the regions inside ($\rho < a$) and outside ($\rho > a$) the loop, with

$$\begin{aligned} b_{h,k,n}^{(<)}(z) &= r_{k,n}(z)\left[\lambda_{k,n}(z)\right]^{1-h} K_1\left[\lambda_{k,n}(z)a\right], \\ b_{h,k,n}^{(>)}(z) &= r_{k,n}(z)\left[-\lambda_{k,n}(z)\right]^{1-h} I_1\left[\lambda_{k,n}(z)a\right], \end{aligned} \tag{18}$$

and

$$C_{h,k,n}^{(<)}(\rho,z) = I_h\left[\lambda_{k,n}(z)\rho\right], \qquad C_{h,k,n}^{(>)}(\rho,z) = K_h\left[\lambda_{k,n}(z)\rho\right]. \tag{19}$$

Expressions (17)–(19) tell us that the distributions of the EM field components at each z-plane are described by linear combinations of modified Bessel functions, of the first or second kind depending on whether the distance ρ of the observation point from the loop axis is smaller or greater than the loop radius a. In particular, the behavior of $K_h\left(\lambda_{k,n}\rho\right)$ as ρ increases satisfies the radiation condition, which demands that the energy radiated by the source to distant observation

points is outgoing and bounded [38–44]. Use of (17) in (1) leads to

$$E_\varphi(\rho,z) = -j\omega\mu_0 Ia \sum_{n=1}^{N_1} b_{1,1,n}^{(\gtrless)}(z) C_{1,1,n}^{(\gtrless)}(\rho,z), \tag{20}$$

$$H_\rho(\rho,z) = -Ia \sum_{n=1}^{N_2} b_{1,2,n}^{(\gtrless)}(z) C_{1,2,n}^{(\gtrless)}(\rho,z), \tag{21}$$

$$H_z(\rho,z) = Ia \sum_{n=1}^{N_1} b_{0,1,n}^{(\gtrless)}(z) C_{0,1,n}^{(\gtrless)}(\rho,z). \tag{22}$$

The solutions in the two regions must match at $\rho = a$. Thus, continuity of E_φ implies the equation

$$\sum_{n=1}^{N_1} b_{1,1,n}^{(<)}(z) C_{1,1,n}^{(<)}(a,z) = \sum_{n=1}^{N_1} b_{1,1,n}^{(>)}(z) C_{1,1,n}^{(>)}(a,z), \tag{23}$$

which is satisfied for any value of the coefficients $r_{1,n}$ and $\lambda_{1,n}$ $(n = 1,\ldots,N_1)$, as can be easily verified. Even the condition $H_\rho(\rho \to a^-, z) = H_\rho(\rho \to a^+, z)$ holds independently of the values assumed by the $r_{2,n}$'s and $\lambda_{2,n}$'s.

Instead, from the continuity of H_z at $\rho = a$ follows that

$$\sum_{n=1}^{N_1} b_{0,1,n}^{(<)}(z) C_{0,1,n}^{(<)}(a,z) = \sum_{n=1}^{N_1} b_{0,1,n}^{(>)}(z) C_{0,1,n}^{(>)}(a,z), \tag{24}$$

which, by making use of (18) and (19), becomes

$$\sum_{n=1}^{N_1} K_1[\lambda_{1,n}(z)a]\, I_0[\lambda_{1,n}(z)a] = -\sum_{n=1}^{N_1} I_1[\lambda_{1,n}(z)a]\, K_0[\lambda_{1,n}(z)a]. \tag{25}$$

The satisfaction or not of this condition depends on the choice of the $\lambda_{1,n}$'s. This means that the numerical discrepancy between left- and right-hand sides of (25) is an index of the goodness of fitting. The more the approximation (12) corresponding to $k = 1$ is refined, the nearer to each other will be the two sides of (25). Thus, an indication about the accuracy of the method can be obtained by checking for the continuity of H_z at $\rho = a$. This will be done in an example in Section 3.

It should be noticed that the developed method does not require that the poles $p_{k,n}$ to be extracted have negative real part, and this constitutes an advantage with respect to the previous pole-residue based approach for solving integral transforms similar to (2) [15], which obliges the fitting algorithm to start a new iteration whenever

the current set of poles is unsuitable and must be discarded, with unavoidable increase of computational time.

Moreover, as the fitting procedure allows users to specify the upper bound for the root-mean-square (RMS) relative error of the rational approximation to be generated [33–35], the numerical results achieved with the proposed method are as accurate as desired within the machine-precision tolerance.

In some cases of geophysical interest, the loop source can be treated as a vertical magnetic dipole (VMD), since its diameter is small if compared to both the source-receiver distance and the free-space wavelength. For instance, this is the case of the radiation from a dipole antenna probe in presence of a lossy ground, which can be used for sensing underground objects or inhomogeneities of other kind [45–49]. In particular, when the soil properties do not vary spatially, the presence of shallow buried objects such as mines, metals, or mineral resources can be detected by the departure of the measured EM field from the one calculated regarding the ground as a homogeneous conducting half-space [9, 45].

The explicit expressions for the relevant EM field components produced by a VMD placed at height t above the top surface of the half-space are derived from (21), (22), and (23) under the assumption of small loop, that is by retaining only terms with the superscript plus (since $a \ll \rho$) and applying the small-argument approximation

$$I_1 \left[\lambda_{k,n}(z)a\right] \cong \frac{\lambda_{k,n}(z)a}{2}, \tag{26}$$

as done in [27, 50, 51]. It yields

$$b^{(>)}_{h,k,n}(z) \cong -\frac{a}{2} r_{k,n}(z) \left[-\lambda_{k,n}(z)\right]^{2-h}, \tag{27}$$

and, consequently,

$$E_\varphi(\rho, z) \cong -\frac{j\omega\mu_0 IA}{2\pi} \sum_{n=1}^{N_1} r_{1,n}(z)\lambda_{1,n}(z) K_1\left[\lambda_{1,n}(z)\rho\right], \tag{28}$$

$$H_\rho(\rho, z) \cong -\frac{IA}{2\pi} \sum_{n=1}^{N_2} r_{2,n}(z)\lambda_{2,n}(z) K_1\left[\lambda_{2,n}(z)\rho\right], \tag{29}$$

$$H_z(\rho, z) \cong -\frac{IA}{2\pi} \sum_{n=1}^{N_1} r_{1,n}(z)\lambda^2_{1,n}(z) K_0\left[\lambda_{1,n}(z)\rho\right], \tag{30}$$

where $A = \pi a^2$, and IA is the dipole moment.

3. RESULTS AND DISCUSSION

Before starting the discussion, the reader should note that the emphasis in this paper is the proposition of a technique for fast calculating the forward solution (1–2), not that of a new method of inversion. When inverting EM data, solving fast the forward problem permits to save computational time at each iteration of the chosen inversion algorithm, whatever it is (see, for instance, the damped least-squares Levenberg-Marquardt method [11]).

In order to test the validity of the developed theory, the amplitude of the EM field components generated on the surface of a two-layer earth by a circular loop carrying 1 A of current is computed. It is initially assumed that $\mu_1 = \mu_2 = \mu_0$, $\epsilon_1 = \epsilon_2 = 10\epsilon_0$, $\sigma_1 = 0.01\,\mathrm{S/m}$, $\sigma_2 = 0.3\,\mathrm{S/m}$, $a = 5\,\mathrm{m}$, $t = 2\,\mathrm{m}$, $d = 10\,\mathrm{m}$, $N_1 = N_2 = 80$. At first, the radial distributions of the field strengths are evaluated at the frequency of 100 kHz. The 3D views depicted in Figs. 2–4 show that

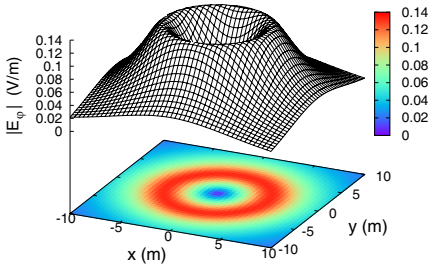

Figure 2. Distribution of the amplitude of E_φ on the surface of a two-layer earth, computed by applying the proposed approach.

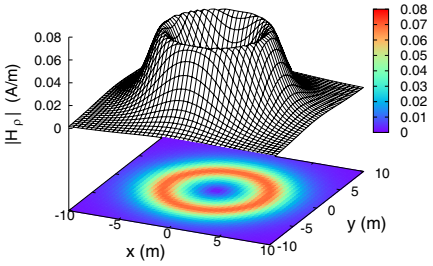

Figure 3. Distribution of the amplitude of H_ρ on the surface of a two-layer earth, computed by applying the proposed approach.

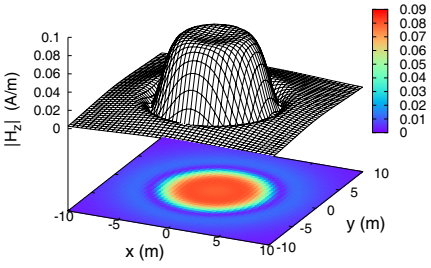

Figure 4. Distribution of the amplitude of H_z on the surface of a two-layer earth, computed by applying the proposed approach.

the maximum amplitudes of E_φ and H_ρ are localized on circular rings approximately below the edge of the loop, while the H_z-field remains confined in the in-loop region. It can be appreciated the continuity of H_z in a neighbourhood of $\rho = a = 5\,\mathrm{m}$, which indicates excellent fitting accuracy according to what has emerged at the end of Section 2. Next, since in most cases inversion of H_z-field measurements is performed, the amplitude of H_z is calculated and plotted against induction number B (i.e., the ratio between the source-receiver distance ρ and the skin depth δ_1 in the top layer) for three distinct values of the thickness d of the top layer. The same medium as in the previous analysis is considered, with $\rho = 100\,\mathrm{m}$, $a = 10\,\mathrm{m}$ and $t = 0$. The obtained results, shown in Fig. 7, are in good agreement with the ones provided by the optimized digital filter operator [12]. Notice that these profiles are computed starting from the determination of a set of eighty-pole rational functions of the form $g_1(z, \lambda)$, each corresponding to a different frequency.

The coefficients of each rational function are determined through an iterative procedure which repeats the execution of the fitting algorithm [33] until the RMS relative error of the generated approximation falls below a user-specified admissible RMS relative error, that is the relative error tolerance threshold `rtol`.

Figure 5 illustrates the computational time taken on a single-core 1.6 GHz Pentium 4 PC to generate one of the rational approximations, as well as the produced RMS relative error, as a function of the tolerance `rtol`. The considered frequency is 100 kHz, even if varying frequency between 1 Hz and 100 kHz is seen to have a negligible effect on the plotted curves.

From the analysis of Fig. 5, it emerges that $N_1 = 80$ poles are sufficient to achieve high accuracy whatever is the desired tolerance. In particular, for `rtol`$= 10^{-4}$ the execution of the procedure terminates after 13 iterations, that is when the RMS relative error of the approximation becomes equal to $4.28 \cdot 10^{-14}$. It turns out that 13 iterations must also be enough to stop the execution of the procedure every time that the admissible error is greater than `rtol`$^* = 4.28 \cdot 10^{-14}$. This explains the piecewise-horizontal trend of the effective relative error in Fig. 5. Conversely, when `rtol`$<$`rtol`* the execution of the procedure cannot last 13 iterations, and 24 iterations are instead necessary in order to get the error below the fixed tolerance. The RMS relative error of the rational approximation obtained after 24 iterations is $5.18 \cdot 10^{-15}$.

It is easily understood how a user, specifying `rtol`, can require a more or less accurate solution. Yet, given the order N_k of approximation of $f^{(k-1)}(z, \lambda)$ $(k = 1, 2)$, there exists a lower bound

for the error tolerance that can be imposed. Choosing `rtol` below such limit therefore means running the fitting algorithm [33] an infinite number of times without finding a solution. However, the lower bound decreases with increasing N_k. This aspect is pointed out in Fig. 6, which shows plots of the RMS relative error of the approximation g_1 versus N_1, with the number of performed iterations I taken as a parameter. Notice that, as I increases, the sequence of curves converges to a limit curve (solid line), which corresponds to $I \geq 10^4$ and represents the locus of the smallest error tolerances that can be reached. Thus, the minimum achievable relative error decreases as the order of approximation of f increases, and asymptotically approaches the machine precision ϵ_{mach}. On the 32-bit computer used for the purposes of this discussion, working in double precision arithmetic, the machine precision (that is the smallest difference between two numbers that the computer can recognize) is equal to $2^{-52} \cong 2.2 \cdot 10^{-16}$ [52, 53].

In Figure 6, it is possible to distinguish three intervals for the choice of N_1, each exhibiting special features. The leftmost region (labelled with 1) includes all the values of N_1 that are smaller than 50, which lead to poor accuracy of approximation (the minimum relative error is at least 10^{-9}) and very fast rate of convergence of the iterative procedure. Moreover, since the slope of the limit curve is approximately constant in the semi-logarithmic scale of Fig. 6, the minimum relative error diminishes exponentially with increasing N_1. The same exponential behavior is maintained in the middle region ($50 \leq N_1 \leq 70$), with the result that the minimum error decreases by five orders of magnitude, from 10^{-9} at $N_1 = 50$ to 10^{-14} at

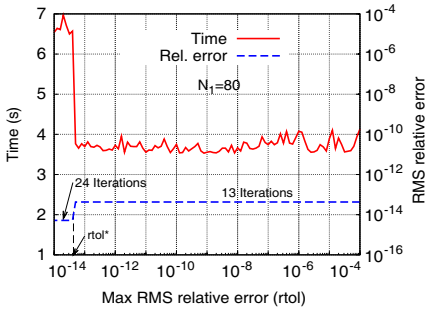

Figure 5. Execution time required to determine the rational approximation $g_1(z, \lambda)$ at 100 kHz, as a function of the admissible RMS relative error.

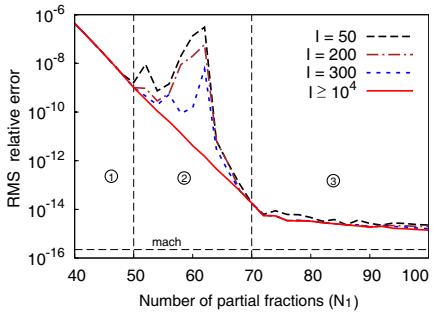

Figure 6. RMS relative error of the rational approximation $g_1(z, \lambda)$ as a function of the order of approximation N_1.

$N_1 = 70$. In particular, starting from $N_1 = 50$ (rough fitting), the addition of any new partial fraction to the rational function series (12) improves significantly the accuracy of approximation, and this happens at the price of an enormous reduction of the convergence rate of the method. It is observed that 10^4 iterations of the fitting algorithm are required in this region to minimize the relative error. When N_1 becomes sufficiently large, say 66 or 68, this latter effect disappears and error-curves associated with different numbers of iterations tend to overlap again. For $N_1 > 70$ (region 3), the technique offers optimal performances in terms of either accuracy and rate of convergence. It is noted that 50 iterations are enough to obtain a RMS relative error smaller than 10^{-14}. However, the slope of the limit curve suffers an abrupt decrease when entering this region, thus implying that the minimum relative error approaches very slowly ϵ_{mach} as N_1 increases.

As to the computational time taken by the developed method, it is expected to be proportional to the required number of iterations. Fig. 5 clearly shows that, for $N_1 = 80$, it is comprised between 3.5 and 4 s (3.7 s on average) or between 6.5 and 7 s (6.7 s on average), depending on whether the number of iterations is 13 or 24. An estimate of the time needed for executing one iteration can be found by dividing each average time by the associated number of iterations. It yields $3.7/13 = 0.285 \cong 6.7/24 = 0.279$ s. The reason for which the cost of each iteration keeps constant while changing `rtol` from 10^{-4} down to 10^{-14} is that it mainly depends on the number of partial fractions N_1 which constitute the rational approximation g_1, as discussed in [33]. Notice that Fig. 5 illustrates the total elapsed time, which includes the CPU-time plus additional minor contributions completely unrelated to the computational work, like the I/O wait. These small contributions cause the elapsed time to fluctuate about the average value.

It has been seen that, correspondingly to `rtol`$>$`rtol`*, the duration of the whole fitting procedure does not exceed 4 seconds. This is the operating condition to be preferred, even if it is not associated with the maximum accuracy (`rtol`$>$`rtol`*ensures 13 digits of precision). As the only time-consuming step of the proposed method is the fitting procedure itself, the calculation of the H_z-field strength takes less than 4 seconds per frequency point.

The new method is thus faster than the previously developed pole-residue based technique described in [15], which takes at least 8 seconds on the same Pentium 4 processor mentioned above. The longer run-time exhibited by the previous algorithm is explained by the fact that, as anticipated in Section 2, it starts a new iteration whenever the real part of one or more of the extracted poles is positive.

Some authors [14] pointed out that designing an optimized digital

filter for evaluating Fourier-Bessel transforms of the type (2) requires about 8 seconds on a 2.4 GHz PC. In principle, this run-time cannot be directly compared with that illustrated in Fig. 5, as a fair run-time comparison of two algorithms is possible only if they are executed on the same computer. On the other hand, to re-implement and run the filter optimization algorithm described in [14] on the same computer used for applying the present method would not be helpful, as there is no guarantee of obtaining an implementation really similar to the original code developed by the authors. For instance, they may have used an efficient data structure or procedure to enhance a critical part of the code, with the result of a substantial saving in computation time.

While in general the execution of two distinct algorithms on different computers renders any precise runtime comparison hard, in the present case it is however possible to conclude that the proposed procedure (task 1) is faster than the digital filter one (task 2). In fact, running the source code of the filter optimization algorithm presented in [14] on a single-core 1.6 GHz Pentium 4 processor would require an execution time $\mathrm{ET}^{(2)}$ that obeys the following constraint

$$\mathrm{ET}^{(2)}_{\mathrm{P4,\,1.6\ GHz}} > \mathrm{ET}^{(2)}_{\mathrm{PC,\,2.4\ GHz}} \cong 8\,s > \mathrm{ET}^{(1)}_{\mathrm{P4,\,1.6\,GHz}}, \tag{31}$$

where the abbreviation PC denotes the computer used in [14]. The first inequality (from the left-hand side) in (31) can be easily verified by comparing the rates of execution, measured in floating-point operations (FLOP) per second, at which a single-core 1.6 GHz Pentium 4 and a wide assortment of 2.4 GHz computers run the so-called LINPACK benchmark programs (see Table 1 in [54] for easy comparison). For instance, the rate of execution of the LINPACK small size problem [54] is 796 MFLOP/s for the 1.6 GHz Pentium 4, a value comprised between 1055 and 1190 MFLOP/s for a generic single-core 2.4 GHz computer. The last inequality in (31) is instead deduced from the results illustrated in Fig. 5.

If it is considered that inversion of CSEM data involves the repeated calculation of forward solutions, time savings resulting from applying the new method rather than the preceding ones is considerable.

When the parameters of the inverted model to be determined are the thicknesses of the various layers, the inversion process is referred to as induction depth sounding (IDS) method. As pointed out in [5, 28], for simple layered earth models like the two-layer one considered in the present analysis, one can deduce the thickness d of the top-layer by directly matching response curves similar to those plotted in Fig. 7 with the recorded experimental data, without resorting to any inversion

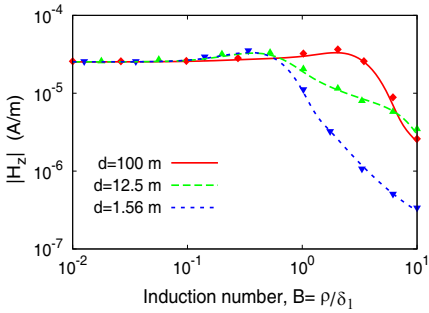

Figure 7. Normalized amplitude of H_z versus induction number, computed on the surface of a two-layer earth model ($\sigma_2/\sigma_1 = 30$). Digital filter ($\bullet$) and proposed ($-$) approaches.

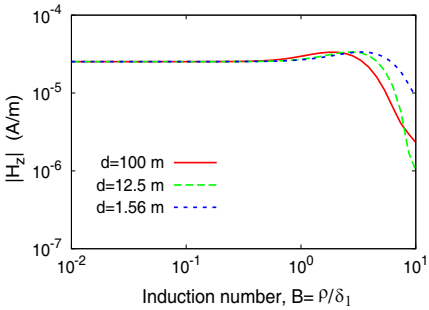

Figure 8. Normalized amplitude of H_z versus induction number, computed on the surface of a two-layer earth model ($\sigma_2/\sigma_1 = 0.3$) by applying the proposed approach.

algorithm. In this case, it is the degree of dissimilarity exhibited by the theoretically computed response curves that permits to interpret the acquired measurements. The more the curves are distinct, the higher is the resolution of IDS. The plots in Fig. 7 demonstrate how, for the particular two-layer earth model considered, measurement of the vertical magnetic field should be made at $B > 0.6$ ($f > 911\,\mathrm{kHz}$) in order to deduce the depth of the electrical discontinuity. The resolution dramatically worsens when using models in which the conductivity contrast σ_2/σ_1 of the layers is less than one (conductivity decreases with depth). This aspect is pointed out in Fig. 8, where H_z-field response curves corresponding to $\sigma_1 = 0.01\,\mathrm{S/m}$ and $\sigma_2 = 0.003\,\mathrm{S/m}$ are plotted.

Notice that the plotted curves do not exhibit a marked dissimilarity, and interpretation is still possible only if the source-receiver distance is at least twice the skin depth δ_1 ($\log(B)>0.3$, $B>2$).

In order to further investigate the effect of varying the conductivity contrast on the magnetic field response over the two-layer structure, profiles of the normalized amplitude of the H_z-field versus frequency are computed for five different values of the conductivity contrast (Fig. 9), with $\sigma_1 = 0.01\,\mathrm{S/m}$, $\rho = 100\,\mathrm{m}$, $a = 50\,\mathrm{m}$, $d = 10\,\mathrm{m}$. The normalization factor is taken to be the vertical magnetic field in free-space (H_z^0). The curves of Fig. 9 show that the free-space solution is not valid over most of the frequency range for $\sigma_2 \gg \sigma_1$, while it holds up to about 10 kHz when $\sigma_2 \ll \sigma_1$. The peak field moves significantly towards higher frequencies as the conductivity σ_2 decreases, with the result that a good resolution of the subsurface layering in terms of

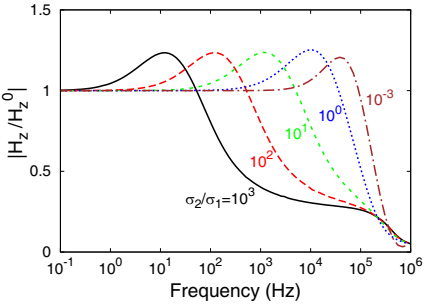

Figure 9. Normalized amplitude of H_z versus frequency with varying the conductivity contrast, computed on the surface of a two-layer earth model by applying the proposed approach.

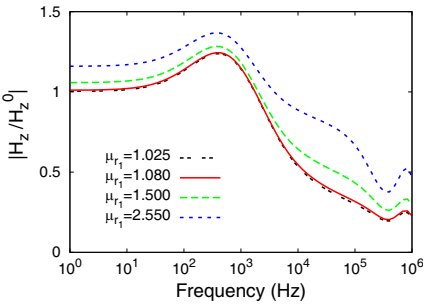

Figure 10. Normalized amplitude of H_z versus frequency with varying the permeability contrast, computed on the surface of a two-layer earth model by applying the proposed approach.

conductivity can be observed.

Since crust is not necessarily nonmagnetic, it may be required to invert even for the magnetic permeability of one or more layers. Thus, sizeable zones of buried magnetically permeable metals or ferrimagnetic minerals, especially magnetite and/or titano-magnetite, distributed in rocks throughout the crust, can be located using simultaneous inversion for conductivity and magnetic permeability [8, 11]. As an example, Figure 10 illustrates the H_z-field response in presence of a two-layer earth model consisting of a 0.01-S/m magnetic layer overlying a nonmagnetic 0.3-S/m half-space, with the permeability contrast $\mu_2/\mu_1 = 1/\mu_{r_1}$ taken as a parameter. Titano-magnetite ($\mu_{r_1} = 2.55$), pyrrhotite ($\mu_{r_1} = 1.5$), basic igneous rocks ($\mu_{r_1} = 1.025$) [55] are the materials considered in this numerical application. The plotted curves evidence an extended, although not pronounced, dissimilarity, even at low frequencies. The observed low-frequency offset from the free-space solution increases with incresing μ_{r_1}, and is to be attributed to the necessity of satisfying the boundary condition of continuity of the vertical magnetic induction B_z across the interfaces between magnetic and non-magnetic layers.

Finally, two more problems are considered for further testing the validity of the developed integration technique, that is those of a large current loop lying on a three-layer earth and a VMD on a homogeneous ground.

In the first case, curves of the H_z-field strength against frequency are computed taking the ratio d_2/d_1 between the thicknesses of the middle and the topmost layers as a parameter, and assuming $\mu_1 = \mu_2 =$

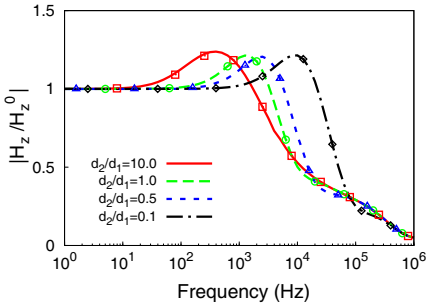

Figure 11. Normalized amplitude of H_z versus frequency, computed on the surface of a three-layer earth model. Digital filter ($\circ$) and proposed ($-$) approaches.

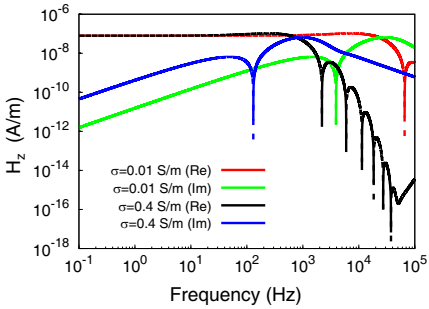

Figure 12. Real and imaginary parts of H_z versus frequency, computed on the surface of a homogeneous earth by applying the proposed approach. Negative (- -) and positive ($-$) values.

$\mu_3 = \mu_0$, $\sigma_1 = 0.01\,\mathrm{S/m}$, $\sigma_2 = 0.3\,\mathrm{S/m}$, $\sigma_3 = 0.001\,\mathrm{S/m}$, $\rho = 100\,\mathrm{m}$, $a = 50\,\mathrm{m}$, $d_1 = 10\,\mathrm{m}$, and $t = 0$. The results achieved by applying the proposed and the digital filter approaches, depicted in Fig. 11, are seen to be substantially overlapping over the whole frequency range of interest.

As for the second problem, expression (30) is used to compute the real and imaginary parts of the H_z-field generated at 100 m from a unit moment VMD on the surface of a 0.01-S/m homogeneous earth. The obtained frequency spectra, presented in Fig. 12, agree well with the ones illustrated in [27]. Notice that increasing σ (up to 0.4 S/m) makes the two spectra shift leftwards, and allows to discover that they exhibit multiple changes in sign, despite what has been asserted in [27]. More in detail, the interval in which the real part of H_z holds the same sign becomes smaller and smaller as frequency increases.

4. CONCLUSION

This paper presents an efficient quasi-analytical procedure for fast solving the forward problem of a large circular current loop located over a layered earth structure. The new procedure reduces the frequency-domain integral representations of the EM field components produced above the medium to expressions involving only a known tabulated Sommerfeld Integral. It involves the rational function-fitting of the parts of the integrands that do not depend on the distance from the loop axis, but, differently from other least squares fitting-based approaches for solving similar transforms, it does not require the

real part of the poles of the generated rational approximations to be strictly negative. It is seen how removing this constraint in the fitting process translates into halving the computational time. Furthermore, the proposed procedure presents advantages even with respect to the commonly used digital filter operators. First, it permits to control the accuracy of the result of the computation, since the maximum admissible RMS relative error produced by the fitting process is a user-defined parameter. On the contrary, the degree of accuracy provided by filters cannot be controlled, and strongly depends on the function to be transformed. Second, it involves a computational cost far less than that implied by the design of optimized filters. Numerical applications are performed in order to validate the method. The achieved results are in fairly good agreement with the data furnished by filter operators.

REFERENCES

1. Boerner, D. E., "Controlled source electromagnetic deep sounding: Theory, results and correlation with natural source results," *Surveys in Geophysics*, Vol. 13, No. 4–5, 435–488, 1992.
2. Zhdanov, M. S., *Geophysical Electromagnetic Theory and Methods*, Elsevier, Amsterdam, 2009.
3. Singh, N. P. and T. Mogi, "EMLCLLER-A program for computing the EM response of a large loop source over a layered earth model," *Computer and Geosciences*, Vol. 29, No. 10, 1301–1307, 2003.
4. Kong, F. N., S. E. Johnstad, and J. Park, "Wavenumber of the guided wave supported by a thin resistive layer in marine controlled-source electromagnetics," *Geophysical Prospecting*, Vol. 29, No. 10, 1301–1307, 2003.
5. Shastri, N. L. and H. P. Patra, "Multifrequency sounding results of laboratory simulated homogeneous and two-Layer earth models," *IEEE Trans. Geosci. Remote Sensing*, Vol. 26, No. 6, 749–752, 1988.
6. Kong, J. A., L. Tsang, and G. Simmons, "Geophysical subsurface probing with radio-frequency interferometry," *IEEE Trans. Antennas Propagat.*, Vol. 22, No. 4, 616–620, 1974.
7. Singh, N. P. and T. Mogi, "Inversion of large loop transient electromagnetic data over layered earth models," *Jour. Fac. Sci Hokkaido Univ. Ser. VII*, Vol. 12, No. 1, 41–54, 2003.
8. Farquharson, C. G., D. W. Oldenburg, and P. S. Routh, "Simultaneous 1D inversion of loop-loop electromagnetic data for magnetic susceptibility and electrical conductivity," *Geophysics*, Vol. 68, No. 6, 1857–1869, 2003.

9. Wait, J. R., "Mutual electromagnetic coupling of loops over a homogeneous ground," *Geophysics*, Vol. 20, No. 3, 630–637, 1955.
10. Constable, S. C., R. L. Parker, and C. G. Constable, "Occams inversion: A practical algorithm for generatlng smooth models from electromagnetic sounding data," *Geophysics*, Vol. 52, No. 3, 289–300, 1987.
11. Beard, L. P. and J. E. Nyquist, "Simultaneous inversion of airborne electromagnetic data for resistivity and magnetic permeability," *Geophysics*, Vol. 63, No. 5, 1556–1564, 1998.
12. Singh, N. P. and T. Mogi, "Electromagnetic response of a large circular loop source on a layered earth: A new computation method," *Pure and Applied Geophysics*, Vol. 162, No. 1, 181–200, 2005.
13. Guptasarma, D. and B. Singh, "New digital linear filters for Hankel J_0 and J_1 transforms," *Geophysical Prospecting*, Vol. 45, No. 5, 745–762, 1997.
14. Kong, F. N., ""Hankel transform filters for dipole antenna radiation in a conductive medium," *Geophysical Prospecting*, Vol. 55, No. 1, 83–89, 2007.
15. Parise, M. and S. Cristina, "High-order electromagnetic modeling of shortwave inductive diathermy effects," *Progress In Electromagnetics Research*, Vol. 92, 235–253, 2009.
16. Alpak, F. O. and C. Torres-Verdin, "Data-adaptive resolution method for the parametric three-dimensional inversion of triaxial borehole electromagnetic measurements," *Progress In Electromagnetics Research B*, Vol. 25, 93–111, 2010.
17. Soleimani, M., "Simultaneous reconstruction of permeability and conductivity in magnetic induction tomography," *Journal of Electromagnetic Waves and Applications*, Vol. 23, No. 5–6, 785–798, 2009.
18. Prasad, R., R. Kumar, and D. Singh, "A radial basis function approach to retrieve soil moisture and crop variables from x-band scatterometer observations," *Progress In Electromagnetics Research B*, Vol. 12, 201–217, 2009.
19. Nordebo, S. and M. Gustafsson, "A priori modeling for gradient based inverse scattering algorithms," *Progress In Electromagnetics Research B*, Vol. 16, 407–432, 2009.
20. Caramanica, F. and G. Oliveri, "An innovative multi-source strategy for enhancing the reconstruction capabilities of inverse scattering techniques," *Progress In Electromagnetics Research*, Vol. 101, 349–374, 2010.

21. Goharian, M., M. Soleimani, and G. R. Moran, "A trust region subproblem for 3D electrical impedance tomography inverse problem using experimental data," *Progress In Electromagnetics Research*, Vol. 94, 19–32, 2009.
22. Zheng, H., M.-Z. Wang, Z. Zhao, and L. Li, "A novel linear EM reconstruction algorithm with phaseless data," *Progress In Electromagnetics Research Letters*, Vol. 14, 133–146, 2010.
23. Chen, X.-D., "Subspace-based optimization method in electric impedance tomography," *Journal of Electromagnetic Waves and Applications*, Vol. 23, No. 11–12, 1397–1406, 2009.
24. Banasiak, R., R. Wajman, D. Sankowski, and M. Soleimani, "Three-dimensional nonlinear inversion of electrical capacitance tomography data using a complete sensor model," *Progress In Electromagnetics Research*, Vol. 100, 219–234, 2010.
25. Mauriello, P. and D. Patella, "A data-adaptive probability-based fast ERT inversion method," *Progress In Electromagnetics Research*, Vol. 97, 275–290, 2009.
26. Cristina, S. and M. Parise, "Fast calculation of theoretical response curves for induction depth sounding," *Proc. of the 39th European Microwave Conference, Sep. 29–Oct. 1, 2009*, 1567–1570, Rome, Italy, 2009.
27. Ward, S. H. and G. W. Hohmann, "Electromagnetic theory for geophysical applications," *Electromagnetic Methods in Applied Geophysics, Theory — Volume 1*, M. N. Nabighian Ed., 131–308, SEG, Tulsa, Oklahoma, 1988.
28. Ryu, J., H. F. Morrison, and S. H. Ward, "Electromagnetic fields about a loop source of current," *Geophysics*, Vol. 35, No. 5, 862–896, 1970.
29. Kong, J. A., *Electromagnetic Wave Theory*, John Wiley & Sons, New York, 1986.
30. Lin, Z., X. Zhang, and G. Fang, "Theoretical model of electromagnetic scattering from 3D multi-layer dielectric media with slightly rough surfaces," *Progress In Electromagnetics Research*, Vol. 96, 37–62, 2009.
31. Gennarelli, G. and G. Riccio, "Diffraction by a lossy double-negative metamaterial layer: a uniform asymptotic solution," *Progress In Electromagnetics Research Letters*, Vol. 13, 173–180, 2010.
32. Dai, S.-Y., C. Zhang, and Z.-S. Wu, "Electromagnetic scattering of objects above ground using MRTD/FDTD hybrid method," *Journal of Electromagnetic Waves and Applications*, Vol. 23,

No. 16, 2187–2196, 2009.

33. Gustavsen, B. and A. Semlyen, "Rational approximation of frequency domain responses by vector fitting," *IEEE Trans. Power Delivery*, Vol. 14, No. 3, 1052–1061, 1999.
34. Gustavsen, B., "Improving the pole relocating properties of vector fitting," *IEEE Trans. Power Delivery*, Vol. 21, No. 3, 1587–1592, 2006.
35. Deschrijver, D., M. Mrozowski, T. Dhaene, and D. de Zutter, "Macromodeling of multiport systems using a fast implementation of the vector fitting method," *IEEE IEEE Microwave Wireless Comp. Lett.*, Vol. 18, No. 6, 383–385, 2008.
36. Gustavsen, B. and C. Heitz, "Modal vector fitting: A tool for generating rational models of high accuracy with arbitrary terminal conditions," *IEEE Trans. Adv. Packaging*, Vol. 31, No. 4, 664–672, 2008.
37. Watson, G. N., *A Treatise on the Theory of Bessel Functions*, Cambridge University Press, 1944.
38. Eroglu, A. and J. K. Lee, "Far field radiation from an arbitrarily oriented hertzian dipole in an unbounded electricaly gyrotropic medium," *Progress In Electromagnetics Research*, Vol. 89, 291–310, 2009.
39. Kudrin, A. V., E. Y. Petrov, G. A. Kyriacou, and T. M. Zaboronkova, "Electromagnetic radiation from sources embedded in a cylindrically stratified unbounded gyrotropic medium," *Progress In Electromagnetics Research B*, Vol. 12, 297–331, 2009.
40. Ruppin, R., "Scattering of electromagnetic radiation by a coated perfect electromagnetic conductor sphere," *Progress In Electromagnetics Research Letters*, Vol. 8, 53–62, 2009.
41. Lamultree, S., C. Phongcharoenpanich, S. Kosulvit, and M. Krairiksh, "Analysis of radiation characteristics of a probe-excited rectangular ring antenna by the dyadic green's function approach," *Progress In Electromagnetics Research B*, Vol. 11, 79–101, 2009.
42. Mushref, M. A., "Radiation from an eccentric coated cylinder with slots of arbitrary sizes and positions," *Progress In Electromagnetics Research B*, Vol. 11, 55–78, 2009.
43. Boriraksantikul, N., P. Kirawanich, and N. E. Islam, "Near-field radiation from commercial cellular phones using a TEM cell," *Progress In Electromagnetics Research B*, Vol. 11, 15–28, 2009.
44. LaComb, J. A., "Spoke top antenna for transient radiation,"

Progress In Electromagnetics Research Letters, Vol. 11, 1–9, 2009.

45. Simons, N. R. S., A. Sebak, and G. E. Bridges, "Application of the TLM method to half-space and remote-sensing problems," *IEEE Trans. Geosci. Remote Sensing*, Vol. 33, No. 3, 759–767, 1995.
46. Parise, M., "Exact electromagnetic field excited by a vertical magnetic dipole on the surface of a lossy half-space," *Progress In Electromagnetics Research B*, Vol. 23, 69–82, 2010.
47. Tiwari, K. C., D. Singh, and M. K. Arora, "Development of a model for detection and estimation of depth of shallow buried non-metallic landmine at microwave x-band frequency," *Progress In Electromagnetics Research*, Vol. 79, 225–250, 2008.
48. Singh, D., N. K. Choudhary, K. C. Tiwari, and R. Prasad, "Shape recognition of shallow buried metallic objects at x-band using ann and image analysis techniques," *Progress In Electromagnetics Research B*, Vol. 13, 257–273, 2009.
49. Kalaee, P. and J. Rashed-Mohassel, "Investigation of dipole radiation pattern above a chiral media using 3D BI-FDTD approach," *Journal of Electromagnetic Waves and Applications*, Vol. 23, No. 1, 75–86, 2009.
50. Lu, Y. L., Y.-L. Wang, Y. H. Xu, and K. Li, "Electromagnetic field of a horizontal electric dipole buried in a four-layered region," *Progress In Electromagnetics Research B*, Vol. 16, 247–275, 2009.
51. Attiya, A. M., "Lower frequency limit of carbon nanotube antenna," *Progress In Electromagnetics Research*, Vol. 94, 419–433, 2009.
52. Muoz-Barrutia, A., X. Artaechevarria, and C. Ortiz-de-Solorzano, "Spatially variant convolution with scaled B-splines," *IEEE Trans. Image Processing*, Vol. 19, No. 1, 11–24, 2010.
53. Higham, N. J., *Accuracy and Stability of Numerical Algorithms*, SIAM, Philadelphia, PA, 2002.
54. Dongarra, J. J., "Performance of various computers using standard linear equations software," Technical report CS-89-85, Department of Computer Science, University of Tennessee, Knoxville, 2008.
55. Telford, W. M., L. P. Geldart, and R. E. Sheriff, *Applied Geophysics*, Cambridge University Press, New York, 1990.